dynamics

MDPI

Article

The In Silico Optimization of a Fed-Batch Reactor Used for the Enzymatic Hydrolysis of Chicory Inulin to Fructose by Employing a Dynamic Approach

Daniela Gheorghe [1], Gheorghe Maria [1,2,*], Laura Renea [1] and Crina Muscalu [1]

[1] Department of Chemical and Biochemical Engineering, University Politehnica of Bucharest, Str. G. Polizu 1-7, 011061 Bucharest, Romania; daniela.corsun@yahoo.ro (D.G.); renea_laura@yahoo.com (L.R.); crina_maria.muscalu@petrom.com (C.M.)
[2] Romanian Academy, Calea Victoriei, 125, 010071 Bucharest, Romania
* Correspondence: gmaria99m@hotmail.com

Abstract: In recent years, inulin enzymatic hydrolysis has become a very promising alternative for producing fructose on a large scale. Genetically modified chicory was used to extract inulin of industrial quality. By using an adequate kinetic model from the literature, this study aimed to determine the optimal operating alternatives of a batch (**BR**) or fed-batch (**FBR**) reactor used for the hydrolysis of inulin to fructose. The operation of the **FBR** with a constant or variable/dynamic feeding was compared to that of the **BR** to determine which best maximizes reactor production while minimizing enzyme consumption. Multi-objective optimal solutions were also investigated by using the Pareto-optimal front technique. Our in-silico analysis reveals that, for this enzymatic process, the best alternative is the **FBR** operated with a constant control variable but using the set-point given by the (breakpoint) of the Pareto optimal front under the imposed technological constraints. This set point reported the best performances, regarding all the considered opposite economic objectives. Also, the **FBR** with a constant, but NLP optimal feeding, reported fairly good performances.

Keywords: inulin hydrolysis to fructose; fed-batch reactor; production maximization; in-silico analysis; Pareto fronts

Academic Editor: Christos Volos

Received: 16 February 2025
Revised: 3 March 2025
Accepted: 4 March 2025
Published: 7 March 2025

Citation: Gheorghe, D.; Maria, G.; Renea, L.; Muscalu, C. The In Silico Optimization of a Fed-Batch Reactor Used for the Enzymatic Hydrolysis of Chicory Inulin to Fructose by Employing a Dynamic Approach. *Dynamics* **2025**, *5*, 10. https://doi.org/10.3390/dynamics5010010

1. Introduction

Biocatalytic processes produce fewer by-products, consume less energy, and generate less environmental pollution, using smaller catalyst concentrations and more moderate reaction conditions compared to classical chemical catalysis [1]. By exhibiting a high selectivity and specificity, they are sustainable bioengineering routes in obtaining a wide range of products and are increasingly replacing some classical processes of fine chemical synthesis [2].

However, a crucial aspect in any realistic engineering analysis for process design, operation, control, and optimization relies on knowledge of an adequate and sufficiently reliable mathematical model of the process [3]. Such valuable kinetic models, based on the reaction mechanism and including key details (e.g., enzyme deactivation), have to ensure interpretable and reliable predictions of the behavior of the enzymatic process under various operating conditions [3–5].

In spite of their large volumes, enzymatic continuously mixed tank reactors, operating in batch (**BR**), or fed-batch (**FBR**) modes, are the most used because they ensure high mass transfer and rigorous temperature/pH control.

Concerning the reactor, an essential engineering problem refers to the development of *optimal operating policies* seeking economic goals, such as production maximization, minimizing raw-material consumption, and obtaining a product of high purity. To address this problem, one engineering approach (developed in this paper) aims to in-silico determine the optimal operating strategy of the reactor that achieves these goals.

In the **BR/FBR** case, its optimal operation problem can be solved **in silico** through two approaches: ***(a)*** **offline** (or 'run-to-run'), with the optimal operating policy being determined using an adequate kinetic model previously identified based on experimental data (this paper) [6–13]; **(b)** ***online***, by using a simplified, often empirical math model to obtain a state-parameter estimator based on the online recorded data (such as the classical Kalman filter) [10,14–21]. One of the **in silico**, *offline* analysis advantages is that it enables a comparison of performances of various bioreactor constructive/operating approaches [22,23].

Even if the enzymatic process (or bioprocess) kinetics and the biocatalyst characteristics (inactivation rate) are known, the in silico solution to this offline engineering problem is not an easy task, due to multiple contrary objectives and a significant degree of uncertainty of the model/constraints originating from multiple sources [14].

In spite of their low productivity, **BRs** are commonly used for slow processes (as is also the case here), because they are highly flexible and easy to operate [24], in various ways [23]: ***(i)*** Simple **BR**, where the substrate(s), biocatalysts, and additives are initially loaded in recommended amounts [2,22,25,26]. Usually, a single- or multi-objective **BR** optimization is performed offline to determine the best batch time and its initial load [14,27,28]. ***(ii)*** Batch-to-batch (**BR**-to-**BR**) optimization, by including a model updating step based on acquired information from past batches (so-called tendency modeling, not used here) to determine the optimal load of the next **BR** [7–9,15,29–34]. ***(iii)*** An optimally operated serial sequence of **BR**s (**SeqBR**) [33], which includes a series of **BR**s of approx. equal volumes. At the end of every **BR,** its content is transferred to the next **BR**, adjusting the reactants and/or biocatalyst(s) concentrations at optimal levels, determined a priori to ensure optimal **SeqBR** operation [9,33]. ***(iv)*** The **s**emi-**b**atch **r**eactor (**SBR)** or fed-batch reactor (**FBR**), with an optimally varied feeding policy of biocatalysts/substrate(s) (not discussed here, see [22,23,35–37]. Usually, **FBR**s report better performances compared to other batch operating alternatives. However, they are more difficult to operate because they need previously prepared stocks of biocatalysts, and substrate(s), of different concentrations (determined a priori in silico), to be fed for every 'time-arc' of the batch (that is, a batch-time division in which the feeding composition is constant and self-understood—the feeding of time-'arcs' usually differs between them) [22,23,38–40]. The time-stepwise variable optimal feeding policy of **SBR**/**FBR** is determined *off-* [23] or *online* [20]. A comparative discussion of all the mentioned bioreactor operating alternatives is provided by Koller [41] and Maria [23].

Fructose is a sweetener of high value in the food and medicine industries. Similar to other polyols largely used as sweeteners (e.g., sorbitol, mannitol, xylitol, erythritol), it is produced on a large scale by using chemical, biochemical, or biological catalysis [42,43].

The **chemical catalytic** hydrogenation of glucose on Ni, Fe, Pt, or Fe-Ni alloy catalysts suffers from a large number of disadvantages: it consumes a lot of energy and occurs at high pressures (10–125 atm) and temperatures (100–140 °C), while the catalyst is very expensive. In addition, the large number of by-products formed during the reaction makes product purification costly [44].

Currently, fructose is produced by the enzymatic **isomerisation of glucose** to fructose on an Fe/CarbonBlack catalyst [43], or over some salts at 50–60 °C and pH = 7–8.5 [45]. The latter starts from the high-fructose syrup (HFCS) obtained from starch [45]. Then, after

rough/fine filtration, ion exchange, and evaporation, a glucose isomerization step can be used to obtain high-fructose syrup (HFS, 42–55% fructose) [45–48]. This process, intensively studied and kinetically characterized, suffers from a series of inconveniences appropriately described in the footnote **[d]** of Table 1.

The biocatalytic routes to produce fructose are more convenient due to a large number of advantages: they consume less energy, by occurring under ambient conditions, and they produce less waste due to their high yield and selectivity, with the product being free of allergenic compounds. A short review of three enzymatic routes to produce fructose at an industrial scale is summarized in Table 1.

The recently developed **two-step Cetus process** (Figure 1, and Table 1) leads to obtaining a high-purity fructose [49–52]. In the first step, D-glucose is converted to keto-D-glucose (kDG) in the presence of pyranose 2-oxidase (P2Ox) and catalase (to avoid the quick inactivation of P2Ox by the H2O2 formed in the main oxidation reaction), at 25–30 °C and pH = 6–7 [22,51]. In the subsequent step, kDG is reduced to D-fructose by NAD(P)H-dependent ALR (aldose reductase, EC 1.1.1.21), at 25 °C and pH = 7 [53], the $NAD(P)^+$ being in-situ or externally regenerated and re-used [54–60]. The process is not yet competitive due to the costly enzymes in both steps.

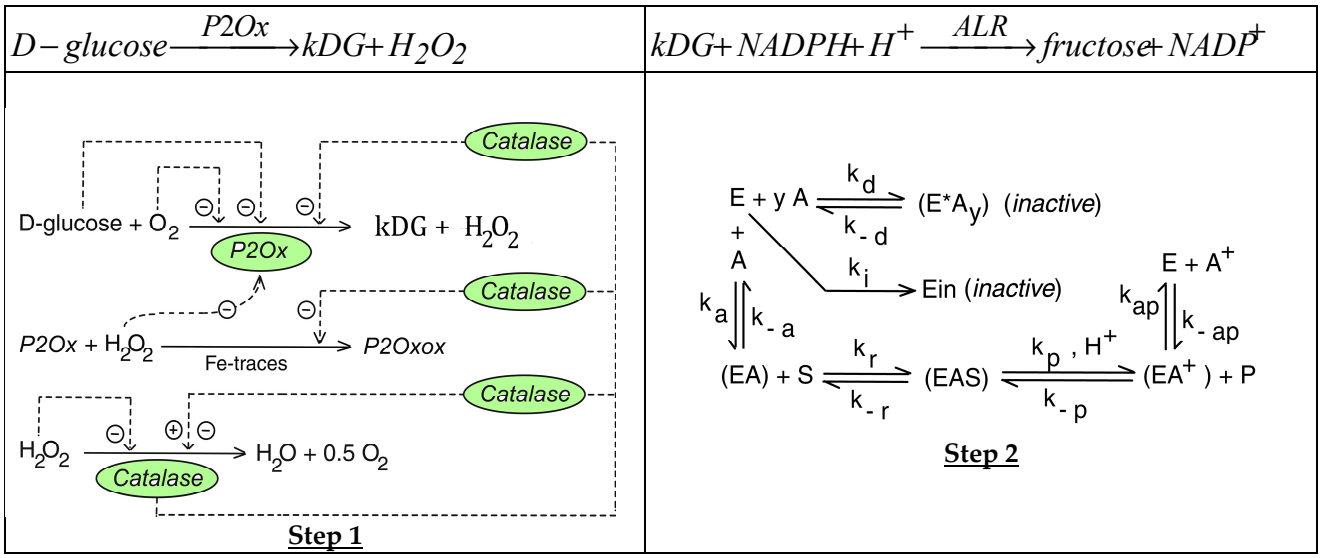

Figure 1. A simplified representation of the two-step Cetus enzymatic process to convert D-glucose to fructose (P). **[Left—Step 1]**. The simplified reaction pathway for D-glucose enzymatic oxidation to keto-D-glucose (kDG or D-glucosone) by using pyranose 2-oxidase (P2Ox) and catalase, proposed by Maria et al. [51]. Perpendicular dashed arrows on the reaction path indicate the catalytic activation, repressing, or inhibiting actions. The absence of a substrate or product indicates an assumed concentration invariance of these species; ⊕/Θ: positive or negative action on reactions. **[Right—Step 2]**. The simplified reaction pathway proposed by Maria and Ene [53] for kDG enzymatic reduction to fructose, by using NADPH and suspended ALR. Notations: E = aldose reductase enzyme (ALR); A = NADPH; S = kDG (substrate); P = fructose (product); Ein, (E^*A_y) = inactive forms of the enzyme. Adapted from [53] with permission from CABEQ Jl.

Another promising biochemical route is the enzymatic **hydrolysis of inulin** (Figure 2). Inulin is industrially extracted from genetically modified chicory crops [61–65], or from modified *Aspergillus* sp. cultures [62,65]. The reported high conversion and selectivity of the hydrolysis process and its simplicity make it a worthy industrial alternative for producing fructose of high quality. Details regarding enzyme purification, and the very high yields realized by the immobilized enzyme are given by [62–65].

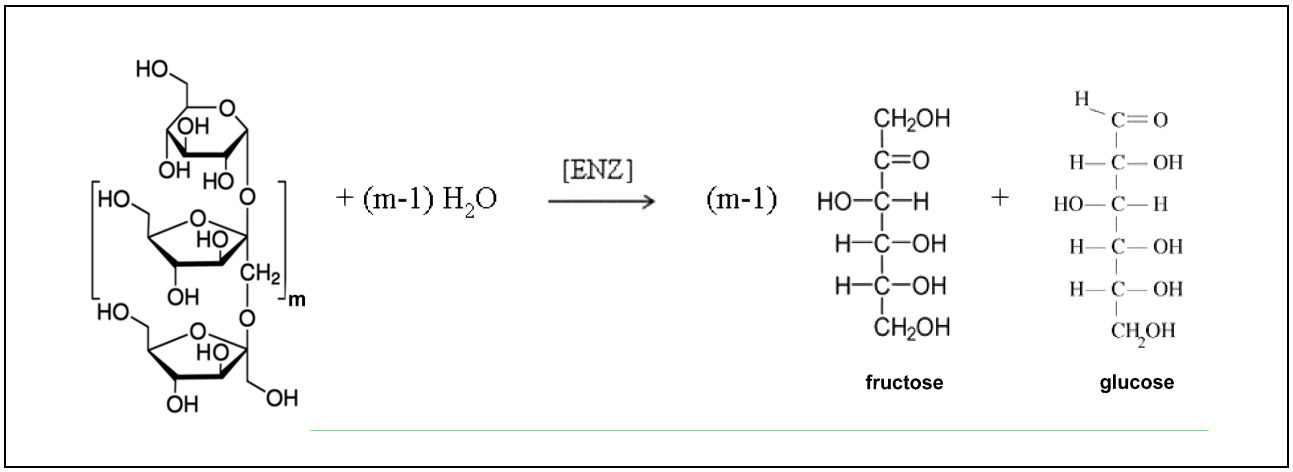

Figure 2. Simplified reaction scheme of hydrolysis of inulin (S) to fructose (F) by using suspended inulinase (E, ENZ). Adapted from [63,64].

In fact, inulin is a polyfructan found in many plants as a storage carbohydrate. It contains up to 70 units of D-fructose linked to terminal glucose, which means that inulin is a mixture of oligomers and polymers [61]. Consequently, inulin is a rich source of fructose, currently used as a macronutrient substitute or as a supplement added to foods. Being a prebiotic, strong interest has been shown in the industrial production of oligofructose and then of fructose from inulin, explaining a large amount of research in this area over recent decades [62–64,66]. The properties of inulin, listed in Table 2, indicate a high solubility, depending on its source, from 60 g/L at 10 °C to 400 g/L at 20–90 °C. However, the recommended concentration in manipulation is a maximum of 100–200 g/L due to its tendency to precipitate and increase solution viscosity [65]. The viscosity of the water solution is close to that of water for concentrations less than 100 g/L (max. 1.0055 cP [67]) but increases sharply for concentrated solutions [68]. Other properties of diluted inulin solutions can be found in the literature, being comparable to those of water (density of, ca., 1.024 g/mL at 55 °C [69]), with a molecular diffusivity of $1.3–1.7 \cdot 10^{-10}$ m^2/s [67,70] for solutions less than 100 g/L. The main component of inulin, fructose, is extremely soluble in water (ca., 22.2 M at room temperature [71]), with diluted solution properties similar to those of water (density of up to 1.1 g/mL [72]), a viscosity up to 1.2 cP [73], and a molecular diffusivity of $1.2 \cdot 10^{-10}$ m^2/s [74] for solutions less than 100 g/L. Only the viscosity increases very sharply for concentrated fructose solutions (more than 600 cP for 70% fructose [71]).

The fructose polymerisation degree in inulin (m) (Figure 2) depends on its origin, being m = 27–29 in commercially available inulin from dahlia, Jerusalem artichoke, or chicory. The content of inulin in plants also varies from 1% in banana, barley, or wheat to, ca., 2–7% in globe artichoke, leek, or onion, and even to, ca., 15–25% in chicory roots, dandelion, garlic, Jerusalem artichoke, and salsify. Genetically improved cultures of chicory might raise the inulin content, making its industrialization attractive for the production of fructose by inulin hydrolysis using inulinase (E.C. 3.2.1.7) [62].

The activity of purified free-inulinase is very high at 50–60 °C and pH = 4–6, but it decreases rapidly at higher temperatures (half-life of $t_{0.5}$ = 17 min at 60 °C compared to $t_{0.5}$ = 34 h at 50 °C [62]). Consequently, several enzyme immobilization alternatives have been searched for, with some being less successful (half-life of $t_{0.5}$ = 138 h at 40 °C and $t_{0.5}$ = 7.2 h at 50 °C in calcium alginate [75]), but others being more promising ($t_{0.5}$ = 21 days at 40 °C and $t_{0.5}$ = 1.1 days at 55 °C on Amberlite support [76]). The thermal stability of the enzyme decreases sharply with temperature, being one of the major causes of activity decay, and running temperatures higher than 60 °C are not recommended.

As another experimental observation, enzyme immobilization significantly decreases its activity. For instance, the fresh-enzyme reaction rate of 0.048 g/L.min is 4× higher than for the immobilized case (on Amberlite support). Immobilization on other supports has also been investigated, e.g., on aminoethylcellulose [77], chitin [78], aminocellulofine beads [79], calcium alginate, agar, gelatin, cellulose [80,81], or macroporous ionic polystyrene beads [82]. In all cases, the enzyme activity decreases several times after immobilization. Some metal ions, such as Hg^{2+} or Ag^{+}, strongly inhibit the enzyme activity, while others (Cu^{2+}, Fe^{3+}) have a little or negligible effect on the free/immobilized enzyme. Various sources of inulinase have been studied, including production from recombinant bacteria [62]. Immobilized inulinase from *K. fragilis* on yeast cells has also been tested, reporting promising results after 30 hrs of batch runs [83].

By adopting an adequate kinetic model from the literature [63,64], and starting from the nominal (non-optimal) operating conditions of Table 2 [63,64,66], the in silico analysis of this study aims to evaluate and compare the performances of several optimal operating policies of a **BR** and **FBR** used for inulin hydrolysis on a free (suspended) inulinase.

Several numerical rules were used in this respect in a novel computational methodology. Thus, the optimal initial load of the **BR**, or the time-stepwise variable feeding policy with multiple control variables of the **FBR**, was determined by using a nonlinear programming (**NLP**) procedure, or a Pareto-optimal front technique, seeking a single-objective optimization (i.e., fructose production maximization), or multiple-objective optimization (i.e., raw-material consumption minimization), in the presence of various technological constraints.

Table 1. Comparison between three enzymatic methods used for fructose synthesis.

Characteristics	Glucose Isomerization [a,d]	Two-Step Cetus Process [b]	Inulin Hydrolysis [c]
Number of steps	1	2	1
Conversion (%)	50 (limited by the equilibrium) [d]	99	99.5
Raw-material availability	Glucose from the starch of crops, molasses, cellulose, and food processing by-products [84]		Genetically modified chicory crop; cultures of *Aspergillus* sp.
Impurities in the product	Yes	Traces	Negligible
Reaction type	Enzymatic isomerization	Enzymatic oxidation (step 1), followed by enzymatic reduction (step 2)	Enzymatic hydrolysis
Enzyme mobility	Immobilized [d]	Free (suspended)	Immobilized
Enzyme stability, and other additives	Intracellular glucose-isomerase (e.g., *Streptomyces murinus*) of low stability; metal (Al) salts	Pyranose 2-oxidase (P2Ox) and catalase (step 1); aldose reductase and NAD(P)H (step 2); enzymes are very costly	Inulinase
Temperature	50–60 °C	25–30 °C (50–60 °C)/ 30 °C	55 °C (40–60 °C)
Reaction time	7 h	3–20 h (step 1); 25 h (step 2)	13 h
pH	7–8.5	6.5–7(−8.5); 7–8.5	5.5
Number of reaction steps	1 isomerization	2 oxidation (step 1), reduction (step 2)	1 hydrolysis
Coenzyme necessary?	No	Yes Catalase for step 1 to prevent P2Ox quick inactivation; NAD(P)H for step 2. NAD(P)H is continuously regenerated in situ	No

Table 1. *Cont.*

Characteristics	Glucose Isomerization [a,d]	Two-Step Cetus Process [b]	Inulin Hydrolysis [c]
Product purification	Difficult **[d]**	Simple (due to high selectivity)	Simple (due to high selectivity)
Product purity	2–5% impurities **[d]**	High (99.9%)	High (99.9%)

[a] Process described by [45,62]. The raw-material HFCS is obtained from yeast hydrolysis (resulting in a mixture of 42% fructose, 50% glucose, and 8% other sugars) [45]. [b] Process described by [49–51,53]; NAD(P)H is continuously regenerated in situ [56]. [c] Process described by [61–64]. [d] This process suffers from a large number of disadvantages: (i) The reaction is thermodynamically limited to around 50% glucose conversion, making the subsequent fructose separation in large chromatographic columns very costly. (ii) Glucose isomerase is an intracellular enzyme with relatively poor stability, making its purification and immobilisation very difficult. (iii) The amylase used to carry out the starch saccharification (to obtain the raw material of HFCS) requires calcium ions for full activity, but calcium inhibits glucose isomerisation, requiring its removal by ion-exchange treatment prior to glucose isomerisation. (iv) The fructose product is still made impure by several other saccharides (such as aldose, which is an allergenic compound) [62,85–89].

Table 2. Nominal operating conditions of the **BR** and its characteristics for the inulin hydrolysis case. Reaction conditions are those of Rocha et al. [66], and Ricca et al. [63,64] [a].

Operating Conditions	Value	Remarks
Reactor liquid volume	1 L (initial)	Up to 10 L capacity
Temperature/pressure/pH (buffer solution)	50–55 °C/normal/4.5–5	Batch time (tf) = 780 min.
Initial concentrations of Ricca et al. [64]	[S]o = 40 (g/L) [E]o = 97 (U/L) [W]o = 988.4 (g/L) [F]o = 0; [G]o = 0	To be optimized within imposed limits (this paper)
Optimization limits of control variables (initial **BR**, or in the **FBR** feeding) [63] [b,c,d]	[S]o; [S]in ∈ [40–200] g/L [E]o; [E]in ∈ [97–5500] (U/L) [W]o ∈ [98–4000] (g) FL ∈ [5 × 10^{-4}–0.01] (L/min)	For **FBR** optimization, the W amount depends on the inlet feed flow rate (FL) of aqueous solution
Fructose polimerization degree in the inulin (m)	29 (adopted)	27–29 Inulin from chicory
Number of time-arcs for the optimized **FBR** (*Ndiv*)	5	**FBR** with variable feeding
Imposed inulin (S) conversion	Min. 90%	
Inulin solubility [b]	60 g/L (10 °C) 160–400 g/L (50 °C), 330 g/L (90 °C)	[62,65,67]
Inulin solution viscosity, density [a]	Comparable to those of water	For [S] < 100 g/L [68,69]
Fructose solubility	4000 g/L (ca., 22.2 M) (25 °C)	https://en.wikipedia.org/wiki/Fructose (last accessing 5 May 2025)
Glucose solution solubility	5–7M (25–30 °C)	[90]
Glucose/fructose solution viscosity	Ca., 1–3 cps (for up to 0.3 M) and 1000 cps (4.5M, 30 °C)	[91]

[a] Physical liquid properties correspond to a solution of inulin (S) and fructose (F), with densities and viscosities given by [72,73,92]. Glucose is present in small concentrations, and its properties were assimilated with those of fructose. Molecular weights: M_F = 180.16 g/mol; $M_S \approx$ 504–5500 g/mol [https://link.springer.com/referenceworkentry/10.1007/978-3-319-03751-6_80-1 (last accessing 5 March 2025)]. [b] Higher concentrations of inlet inulin solution have also been reported (up to 200 g/L [66]). The inulin solubility depends on its source and purification method, varying from 60 g/L at 10 °C to 160–400 g/L at 50 °C, and to more than 330 g/L at 90 °C [62,65]. [c] Maximum enzyme activity is reported as, ca., 3000 U/mL (from *K. marxianus var. marxianus CBS 6556*) and, ca., 58,000 U/g (from *Trametes multicolor* [62]). [d] One unit (U) of inulinase activity is defined as the amount of enzyme necessary to produce 1 µmole of fructose by the hydrolysis of inulin over 1 min of reaction under the standard conditions of 60 °C and pH = 5 [63].

The paper presents a significant number of novelty aspects, as follows: ***(i)*** The engineering evaluation of this process with accounting for several reactor operation alternatives is a premiere in the literature. ***(ii)*** The way by which this difficult multi-objective optimization problem was successfully solved is a model that can be followed to solve similar enzymatic processes. ***(iii)*** The in silico (model-based) engineering analysis of a complex enzymatic process, leading to obtaining a Pareto-optimal operating policy of the approached **BR** is an approach seldom used in the literature. ***(iv)*** Confirmation that the Pareto-front 'break-point' choice proposed technique reported fairly good performances for a **BR**, from

a multi-objectives perspective. ***(v)*** The scientific value of this paper is not *virtual*, as long as the numerical analysis is based on the kinetic model of Ricca et al. [63,64] constructed and validated by using extensive experimental data sets. ***(vi)*** The in-silico analysis suggests that, for this enzymatic process, the best alternative is the **FBR** operated with a constant, but using the set-point given by the (breakpoint) of the Pareto optimal front under technological constraints for the control variables. This set point reported the best performances, regarding all the considered opposite objectives. Also, the **FBR** with a constant, but NLP optimal feeding, reported very good performances.

2. The Experimental Enzymatic Reactor

The **BR** analyzed here was also used by [63,64,66] to study inulin hydrolysis and eventually derive a kinetic model of this process. The characteristics of this **BR** are presented in Table 2, while a reduced scheme is presented by Maria et al. [93]. The reactor includes a large number of components, so its operation is completely automated, with tight control of the pH, temperature, mixing speed, and feeding. Details about the reaction conditions and the control variable ranges are given in Table 2.

In the **BR** operating mode, substrate(s), biocatalysts, and additives are only initially loaded in optimum amounts, to be determined in silico by solving an optimization problem (product maximization here) in the presence of multiple technological constraints.

In the **FBR** operating mode, the substrate(s)/biocatalyst and additives (pH-control substances, etc.) are continuously added during the batch, following a time-stepwise variable (optimal) policy and a variable feed flow rate, to be determined in silico by solving an *offline* optimization problem (this paper and [23,38]) or an *online* one [20]. The **FBR** presents a similar construction to the **BR**, with similar modeling hypotheses. In both cases (**BR** or **FBR**), there is no discharge (effluent) during the batch.

3. Process Kinetics and Reactor Dynamic Model

The main reaction pathway, including the successive enzymatic hydrolysis of inulin, is presented in Figure 2. Based on the experimental data presented in Figure 3 (the blue kinetic curves), collected from a non-optimally operated **BR** of Table 2, using free enzyme, Ricca et al. [63,64] developed a kinetic model of this enzymatic process. This model, presented in Table 3, is able to fairly simulate the dynamics of the key species of the process [abbreviated S, F, W, G, and E] over a long batch (780 min). The differential mass balance of species was formulated by adopting an average fructose polymerisation degree in inulin of $m = 29$.

By using this adequate kinetic model, the in-silico engineering analysis developed here aims to determine the optimal operating strategy of a **BR** or a **FBR**, leading to high yields in fructose, with consuming less free enzyme, under the process conditions of Table 2. (50–55 °C/4.5–5 pH). For this purpose, multiple objectives have been employed, together with several control variables varied over large but feasible domains.

In brief, the enzymatic **BR** model is presented in Table 4 including the mass balances of the key species of the process: [S, F, W, G, E] (Table 3); all of them are observable, with a measurable concentration.

The overall hydrolysis reaction of Table 3 is of a Michaelis–Menten type, with the rate constants depending on the temperature following the classic Arrhenius law. More details about this reaction mechanism are given by Ricca et al. [63,64]. To estimate the rate constants of Table 3, by using the experimental kinetic curves of Figure 3 (blue curves), combined Lineweaver–Burk plots, with an NLP numerical rule, were applied. More details on the estimation procedure used, and on the statistical quality of the estimated rate constants, are given by Ricca et al. [63,64].

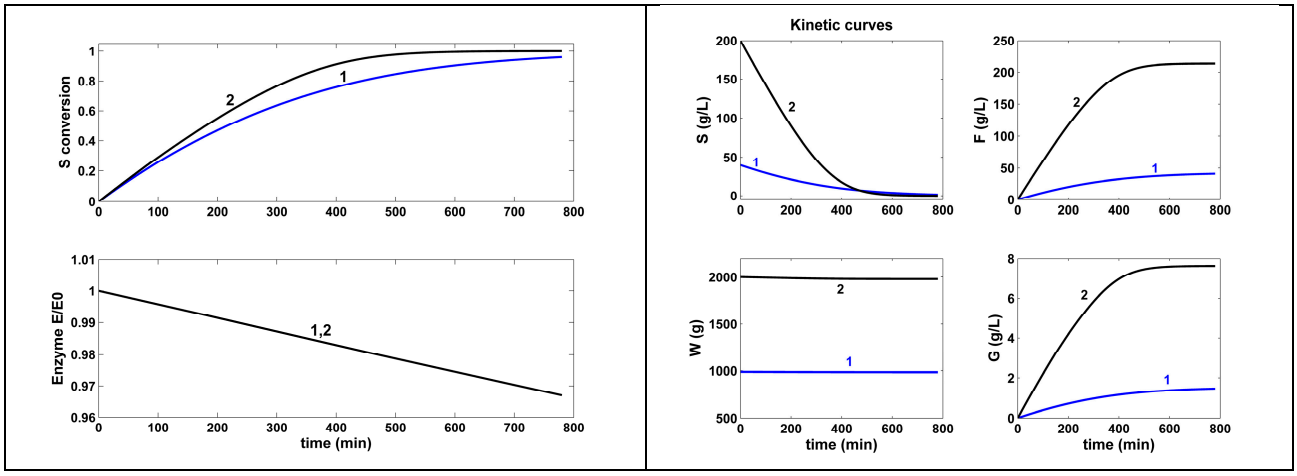

Figure 3. **[Left]** Dynamics of S-conversion and of the relative enzyme activity. **[Right]** Dynamics of the key species of the process in the **experimental** non-optimally operated **BR** of Ricca et al. [64] (**1—blue lines**), compared to the **optimal** NLP-operated **BR** (**2**—simulated **black lines**). Search ranges for the control variables are given in Table 2 and Table 6.

According to Ricca et al. [63,64], a 780 min batch time is sufficient to obtain a high S-conversion (96%) for the nominal (non-optimal) conditions of [S]o = 40 g/L, [E]o = 97 U/L, [W]o = 988 g/L (that is, 1 L), 50 °C, and pH = 5. A wider range of operating conditions was also investigated. Consequently, the feasible ranges of the reactor control variables were set at the values specified in (Table 2).

Table 3. Inulin hydrolysis reaction mechanism, and the reduced kinetic model proposed by Ricca et al. [63,64]. The commercial inulinase used was obtained from *Aspergillus ficuum*. Notations: S = inulin (substrate); F = fructose; W = water; G = glucose; E = enzyme; I_m = inulin with *m*-degree of fructose polymerisation; T = temperature (K); and M = molecular mass (g/mol). Indexes: S = substrate; E = enzyme; W = water; F = fructose; and G = glucose.

Reaction Pathway (Figure 2): $I_m + H_2O \overset{inulinase}{\rightarrow} I_{m-1} + F;\ I_{m-1} + H_2O \overset{inulinase}{\rightarrow} I_{m-2} + F;$ ●●●●● $I_3 + H_2O \overset{inulinase}{\rightarrow} Sucrose + F;\ Sucrose + H_2O \overset{inulinase}{\rightarrow} G + F;$ $I_m + H_2O \overset{inulinase}{\rightarrow} I_{m-q-1} + I_{q+1}$ The above consecutive scheme is approximated by the overall reaction: $S(I_m) + (m-1)H_2O \overset{E}{\rightarrow} (m-1)F + G$	
Rate expressions:[a] $r_S = -\frac{k_2 c_E c_S}{K_m + c_S} = \frac{v_{mS} c_S}{K_m + c_S};\ v_{mS} = k_2 c_E$ $r_F = \frac{dc_F}{dt} = \frac{v_{mF} c_S}{K_m + c_S};\ v_{mF} = \alpha\, v_{mS};$ Or, equivalently, one can write $r_F = -r_S \frac{1}{\frac{m}{m-1} - \frac{M_W}{M_F}}$ $r_W = \frac{dc_W}{dt} = -\frac{v_{mW} c_S}{K_m + c_S};\ v_{mW} = v_{mF} \frac{M_W}{M_F}$ $r_G = \frac{dc_G}{dt} = \frac{v_{mG} c_S}{K_m + c_S};\ v_{mG} = v_{mF} \frac{1}{m-1}$	**Rate constants:** $m = 29;\ M_W = 18$ g/mol $M_F = M_G = 180$ g/mol $k_2 = exp(23.22 - 9450/T)$, g/U·min **[b]** $K_m = exp(27.4 - 7630/T)$, g/L $\alpha = \frac{1}{m/(m-1) - M_W/M_F}$
T is better to keep it. Enzyme deactivation model: - Adopted first-order model: $r_E = k_d c_E,\ \Rightarrow\ c_E = c_{Eo} exp(-k_d t)$ Or, equivalently, one can write $r_E = \frac{dc_E}{dt} = -k_d E$	$k_d = exp(125 - 42300/T)$, 1/h (experimental, free enzyme)
- Other data from the literature: Free enzyme [75] Immobilized enzyme [75]	$k_d = exp(183.64 - 61440/T)$, 1/min $k_d = exp(109.22 - 36025/T)$, 1/min
- Other rate expressions (pseudo-second-order, not tested here): $r_E = k_d c_E (c_E / c_{Eo}),\ \Rightarrow\ c_E = c_{Eo}/(1 + k_d t)$ Free enzyme [76] Immobilized enzyme [76]	$k_d = exp(41.8 - 14599/T)$, 1/h $k_d = exp(49.4 - 17374/T)$, 1/h

Footnotes: [a] c_S, c_F, c_W, and c_G are in g/L; c_E is in U/L; and r_j is in g/L·min. [b] The pre-exponential factor [exp(21.4)] was modified by Maria [22] to [exp(23.22)] to better match the experimental kinetic plots of Ricca et al. [64].

Table 4. Mass balances of key species in the BR model by including the kinetic model of the enzymatic process together with the associated rate constants of Table 3. The ideal model hypotheses of Maria [23], Moser [94], and Dutta [95] assume a homogeneous liquid composition, with negligible mass transport resistance in the bulk phase.

Species	Remarks
Species mass balances: $\frac{dc_j}{dt} = \sum_{i=1}^{n_r} \nu_{ij}\, r_i(\boldsymbol{C}(t), \boldsymbol{C_o}, \boldsymbol{k})$; 'j' = species index (S, F, W, G, E), With the initial conditions of $c_{j,o} = c_j(t=0)$, where 'i' = (S, E, W) are to be optimized; $c_{j,o}$= 0, for j = (F, G).	The species reaction rate (r_i) expressions, the rate constants, and the stoichiometry (ν_{ij}) are given in Table 3. Enzyme (E) deactivation is included in this dynamic balance. The optimal initial load of the **BR** (Table 6) is determined *offline* by solving in silico the associated NLP optimization problem (this paper). $\boldsymbol{C}$ = species concentration vector; $\boldsymbol{k}$ = rate constants vector.

Table 5. Mass balances of key species in the fed-batch bioreactor **FBR** model by including the kinetic model of the enzymatic process together with the associated rate constants of Table 3. The ideal model hypotheses of Maria et al. [96] assume a homogeneous liquid composition by neglecting the mass transport resistance in the bulk phase. The time-stepwise variable feeding is made over Ndiv time arcs (adopted Ndiv = 5 here), where Ndiv is the number of equal time arcs, in which the batch time (tf) is divided. The control variables are $C_{S,inlet,j}$, $C_{E,inlet,j}$, and $F_{L,j}$, with j = 1, . . . Ndiv.

Species	Remarks
Species mass balances: $\frac{dC_i}{dt} = \frac{F_{L,j}}{V_L}\left(C_{i,inlet,j} - C_i\right) \pm r_i(\boldsymbol{C}(t), \boldsymbol{C_o}, \boldsymbol{k})$; $C_{i,o} = C_i(t=0)$, for species '' = S, F, G, E; $C_{i,o} = C_{i,inlet,1}$, for '' = S, E; $C_{i,inlet,j}$, $F_{L,j}$= control variables. '' = S,E; 'j' = 1,.., N_{div}; unknown time-stepwise values to be determined from the **FBR** optimization. For species W, the mass balance is **[b]** $\frac{dW}{dt} = \frac{F_{L,j}}{V_L}(-W) + r_w(\boldsymbol{C}(t), \boldsymbol{C_o}, \boldsymbol{k}) + F_{L,j}\rho_W$ [W]o = 988 g/L; $c_{j,o}$= 0, for 'j' = (F, G).	For the optimal **FBR** with the adopted N_{div} = 5, the feeding policy is (Footnote **[a]**) $\left[C_{S,inlet}\ ;\ C_{E,inlet}\right] = \begin{cases} \left[C_{S,inlet,1}\ ;\ C_{E,inlet,1}\right] \text{ if } 0 \le t < \text{T1} \\ \left[C_{S,inlet,2}\ ;\ C_{E,\text{inlet},2}\right] \text{ if T1} \le t < \text{T2} \\ \left[C_{S,inlet,3}\ ;\ C_{E,inlet,3}\right] \text{ if T2} \le t < \text{T3} \\ \left[C_{S,inlet,4}\ ;\ C_{E,inlet,4}\right] \text{ if T3} \le t < \text{T4} \\ \left[C_{S,inlet,5}\ ;\ C_{E,inlet,5}\right] \text{ if T4} \le t \le \text{T5} = t_f \end{cases}$
Liquid volume in the reactor (footnote [c]): $\frac{dV_L}{dt} = F_{L,j}$; $F_{L,j}$= control variable; 'j' = 1, ..., N_{div}; unknown time-stepwise values to be determined from the **FBR** optimization. The unknown $F_{L,0} = F_L(\text{t} = 0) = F_{L,1}$ is determined together with all the $F_{L,j}$ values.	For the optimal **FBR** with the adopted N_{div} =10, the feeding policy is (Footnote **[a]**) $F_{L,j} = \begin{cases} F_{L,0} \text{ if } 0 \le t < \text{T1} \\ F_{L,1} \text{ if T1} \le t < \text{T2} \\ F_{L,2} \text{ if T2} \le t < \text{T3} \\ F_{L,3} \text{ if T3} \le t < \text{T4} \\ F_{L,4} \text{ if T4} \le t \le \text{T5} = t_f \end{cases}$

Footnotes: [a] For the adopted N_{div} = 5, the j = 1, …, N_{div} time-arc switching points are as follows: T1 = t_f / N_{div} = 156 min; T2 = 2 × T1; T3 = 3*T1; T4 = 4*T1; and T5 = t_f = 780 min. [b] The water density is ρ_W = 988 g/L (50 °C). [c] The $F_{L,j}$ time-stepwise feed flow rates are determined simultaneously with the other control variables (that is, $C_{E,inlet,j}$ and $C_{S,inlet,j}$) to ensure optimal FBR operation.

4. Optimization Problem for BR and FBR

4.1. Selection of Control Variables

By analyzing the dynamic models of **BR** and **FBR** of Tables 4 and 5**,** respectively, the chosen control variables are those related to the initial reactor load or its variable feeding:

BR case: Initial load of [S]o, [E]o, and [W]o (substrate, enzyme, and water, respectively).
FBR case: The feed characteristics for every time-division (arc), that is, $C_{S,inlet,j}$, $C_{E,inlet,j}$, and $F_{L,j}$, with j = 1, . . ., Ndiv (number of equal time arcs in which the batch time is divided).

4.2. NLP Optimization with a Single Objective Function (Ω)

Optimization of a **BR** operation translates to finding its initial load with the key species mentioned in Section 4.1 (that is, three unknowns in the present case, see the Table 4), by using a common nonlinear programming (**NLP**) optimization rule, seeking to determine the extreme of an objective function in the presence of multiple constraints. In the present case, this problem refers to the maximization of [**F**] (fructose) production:

$$\begin{aligned} &\text{Given [F]o = 0 and [G]o = 0,} \\ &\text{find control variables [S]o, [E]o, and [W]o such that} \\ &\text{Max } \boldsymbol{\Omega}(\boldsymbol{C}, \boldsymbol{C_o}, \boldsymbol{k}), \text{ where } \boldsymbol{\Omega} = [\mathbf{F}(t)] \end{aligned} \tag{1A}$$

For the **FBR** case, the batch time is divided into Ndiv equal time- arcs (Ndiv = 5 adopted here). The control variables $C_{S,inlet,j}$, $C_{E,inlet,j}$, and $F_{L,j}$, with j = 1, …, Ndiv, are kept constant over every time-arc at optimal values to be determined by solving the optimization problem shown in Equation (1B), with using the model of Table 5. The self-understood control variables may differ between different time-arcs. The time intervals of equal lengths $\Delta t = t_f/\mathbf{N_{div}}$ are obtained by dividing the batch time t_f into $\mathbf{N_{div}}$ parts $t_{j-1} \leq t \leq t_j$, where $t_j = j \cdot \Delta t$ are switching points (where the reactor input is continuous and differentiable) [20,22,23,38,39,93,96]. In the present case, the switching points are presented explicitly in Table 5.

$$\begin{aligned} &\text{Given [F]o = 0 and [G]o = 0, find the following control variables:} \\ &C_{S,inlet,j}, C_{E,inlet,j}, \text{ and } F_{L,j}, \text{ B} \\ &\text{for j = 1, …, } \mathbf{N_{div}}\text{, with the adopted } \mathbf{N_{div}} = 5 \text{ time-arcs, and the initial } \underline{\mathbf{FBR}} \text{ condition of Table 5, to obtain} \\ &\text{Max } \boldsymbol{\Omega}(\boldsymbol{C}, \boldsymbol{C_o}, \boldsymbol{k}), \text{ where } \boldsymbol{\Omega} = [\mathbf{F}(t)] \end{aligned} \tag{1B}$$

The optimal **FBR** principle indicates obtaining an optimal feeding policy consisting of a time-stepwise variation in the control variables (i.e., feeding liquid flow rate and the concentrations of the added substrates and biocatalyst) over the adopted $\mathbf{N_{div}} = 5$ equal 'time-arcs' of the batch [23,96]. This implies dividing the batch time into equal $\mathbf{N_{div}}$ time-'arcs', with the feeding being constant over each time-arc, but at different values between them. The suitable choice of a small $\mathbf{N_{div}}$ is discussed by Maria [23].

In Equation (1A,B), the time-varying [**F**(*t*)] is a multi-variable function $F(\boldsymbol{C}(t),\boldsymbol{C_o},\boldsymbol{k})(t)$, evaluated by using the process/reactor model of Tables 4 and 5, respectively, over the whole batch time $(t) \in [0, t_f]$. As an observation, Figures 3, 4A and 5A reveal that, in the present case study, the maximum **[F]** is reached at the batch end. Notations: $\boldsymbol{C}$ = species concentration vector; $\boldsymbol{C_o}$ = initial value of $\boldsymbol{C}$; $\boldsymbol{k}$ = kinetic model rate constant vector.

As an observation, other optimization objectives can be applied as well, such as a multi-objective one [39,56]. However, the adopted single-objective optimization, seeking the main goal, presents the advantage of simplicity and easy application and interpretation.

The **[F(*t*)]** time-evolution is determined by solving the reactor dynamic model of Table 4, or Table 5 over the whole batch time $(t) \in [0, t_f]$, with the initial condition of $C_{j,0} = C_j(t = 0)$ searched during the optimization iterative numerical rule. The dynamic model solution was obtained with enough precision by using the low-order stiff integrator (ode15s) of the MATLAB computational package.

4.3. Optimization Problem Constraints

The nonlinear optimization problem (**NLP**) formulated above, Equations (1A) or (1B), must account for the following constraints:

(a) The **BR** model of Table 4 including the process kinetic model (Table 3);
(b) The **FBR** model of Table 5, including the process kinetic model (Table 3);

(c) To limit the excessive consumption of raw materials, feasible searching ranges are imposed on the control/decision variable, as stipulated in Table 2.

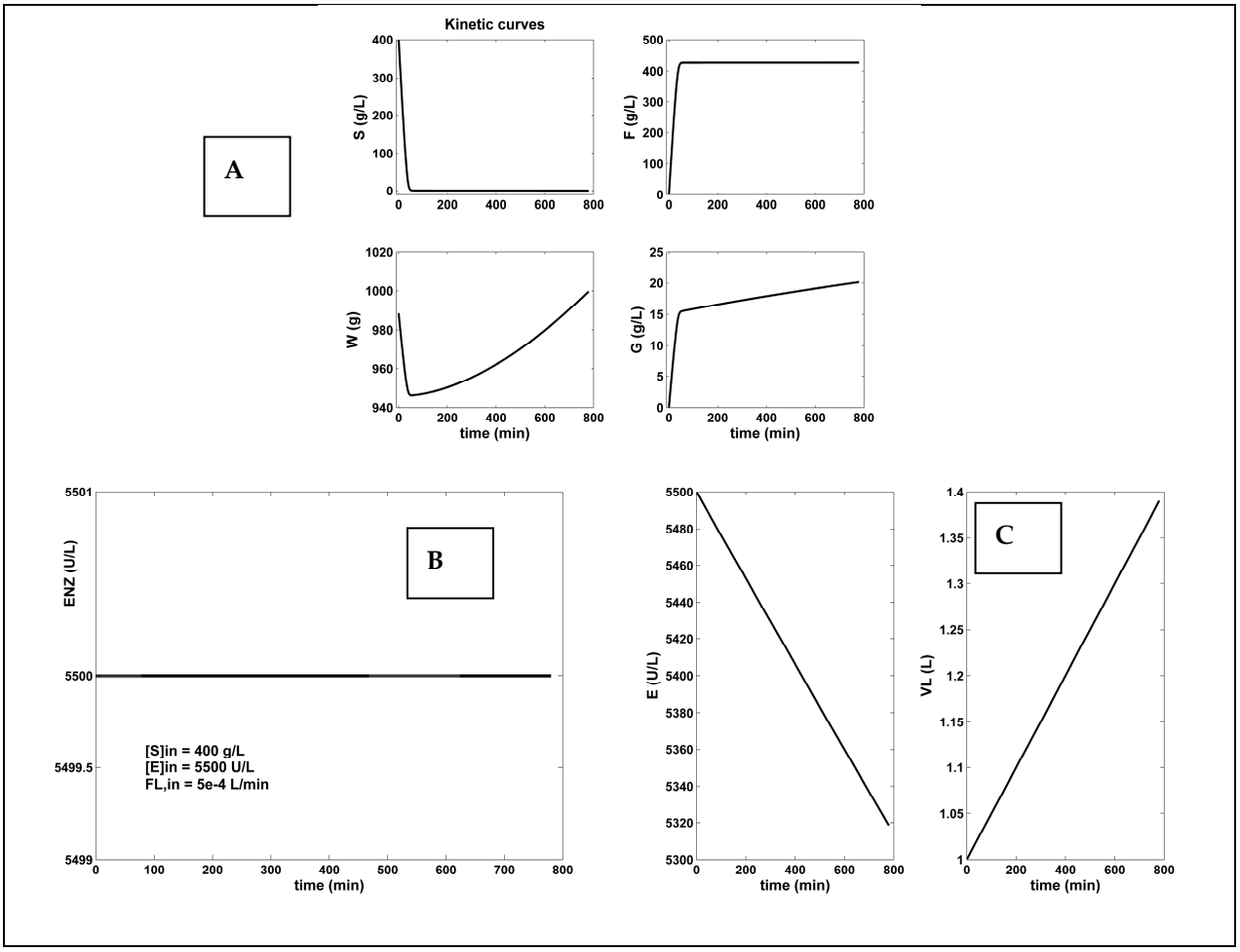

Figure 4. [**Figure [A]**] Simulated species concentration dynamics for the **FBR** with a **constant** but optimal NLP feeding. [**Figure [B]**] The optimal constant feeding with enzyme [E]in, substrate [S]in, and feed flow rate FL,in. [**Figure [C]**] Enzyme dynamics in the reactor bulk, and the increase in liquid volume. The search ranges of control variables are given in Tables 2 and 6. The optimal constant feeding rates are [E]in = 5485.2 U/L, substrate [S]in = 400 g/L, and feed flow rate FL, in = 5.13×10^{-4} L/min.

To be considered in the optimization problems, Equation (1A) or (1B), these constraints should be 'translated' to a mathematical form. Eventually, the resulting **NLP** optimization problem is highly non-convex and nonlinear, being subjected to the following technological/physical meaning/model constraints:

Nonlinear process and reactor model:

Table 4 for the **BR** case.
Table 5 for the **FBR** case. (2i)

Physical significance constraints:

$c_j(t) \geq 0$, in Table 4 and Table 5, for all the species of index 'j' and for all $t \in [0\text{-}t_f]$ (2ii)

Searching ranges for the control variables are given in Table 2:

[S]o; [S]in ∈ [40–400] g/L
[E]o; [E]in ∈ [97–5500] (U/L) (2iii)
[W]o ∈ [988–4000] (g)
FL ∈ [5×10^{-4}–0.01] (L/min)

$$V_L \leq 10 \text{ L (reactor capacity)} \quad (2iv)$$

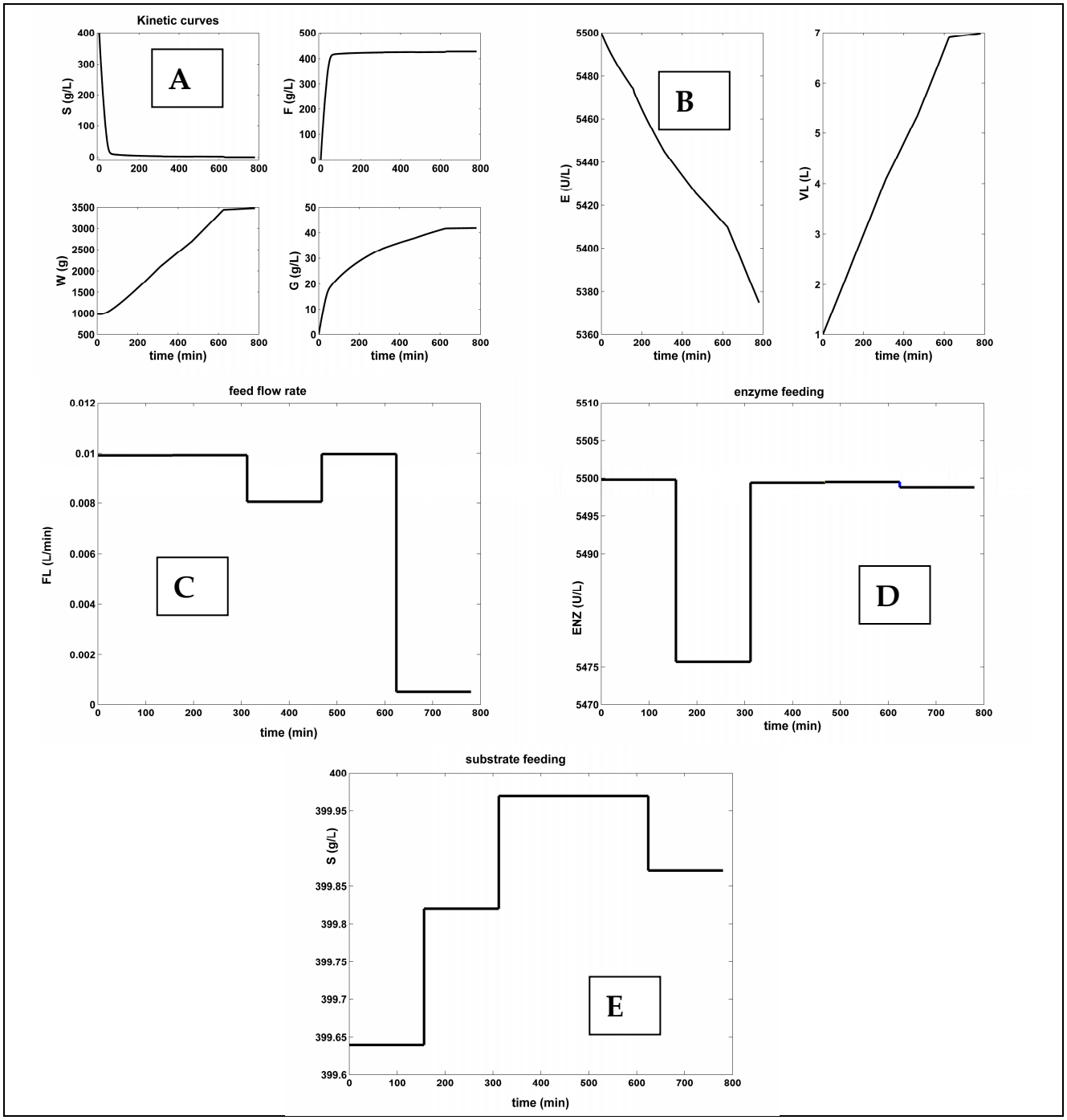

Figure 5. [Figure [A]] Simulated species concentration dynamics for the **FBR** with a **variable** but optimal NLP feeding. **[Figure [B]]** Enzyme dynamics in the reactor bulk, and the increase in liquid volume. **[Figure [C]]** The optimal variable feeding with feed flow rate FL,in. **[Figure [D]]** The optimal stepwise variable feeding with enzyme [E]in. **[Figure [E]]** The optimal stepwise variable feeding with substrate [S]in. The search ranges of control variables (FL,in; [S]in; [E]in) are given in Table 6.

4.4. Pareto-Optimal Front Optimization with Opposite Objective Functions

When multiple opposite objective functions are formulated for an optimization problem, an elegant alternative is to use the Pareto-optimal front technique. Each Pareto-optimal front (curve) accounts for two opposite optimization objectives.

Following the Pareto-front definition [97], any running point from the Pareto-curve can be a valid solution to the optimization problem. With the Pareto-curve being a continuous one, when two opposite optimization criteria are used, an infinity of Pareto-optimal operating solutions can exist. Consequently, the chosen solution (that is, the optimal operation set-points of the **FBR** here) is subjective and case-dependent, and it should be chosen by adding a criterion not accounted for when the Pareto-front was generated. It should be noted that many Pareto-fronts of different shapes can exist for the same optimization problem [93].

In the present case study, by analyzing the **FBR** model of Table 5 and its control variables, at least three Pareto fronts can be found for the case of *constant optimal feeding*, as presented in Equation (3). Additional objectives can exist, but the present analysis was limited to the following ones.

$$\begin{matrix}\text{Maximum F production vs. minimum substrate (S) consumption.}\\ \text{Minimum constant feed flow rate for various maximum F produced.}\\ \text{Maximum F production vs. minimum enzyme (E) consumption.}\end{matrix} \quad (3)$$

As the literature reveals [97], a lot of Pareto-optimal fronts are monotonous and of an exponentially/logarithmic-like shape. Extended studies of [39,56,98] for such kind of shapes, made on various (bio)chemical reacting systems, indicated that the 'break-point' of the Pareto-front (Figures 6 and 7 in the present case) is a good choice for the optimization problem with at least two opposite objectives. As recommended, this 'break-point' should be, ca., 5% higher on the ordinate than the 'baseline' of the Pareto-curve. This is because a running point on the baseline (on the left of the 'break-point' in Figure 6) is not economic, by reporting a lower production of the target product; on the contrary, a running point chosen on the right of the 'break-point' reports a higher productivity, but with the cost of an increasingly higher enzyme consumption, and a violation of the technological constraints (Equation (2)). In the present case, the chosen 'break-point' of Figures 6 and 7 is presented in Table 6 and reports better performances compared to other **FBR** operating alternatives.

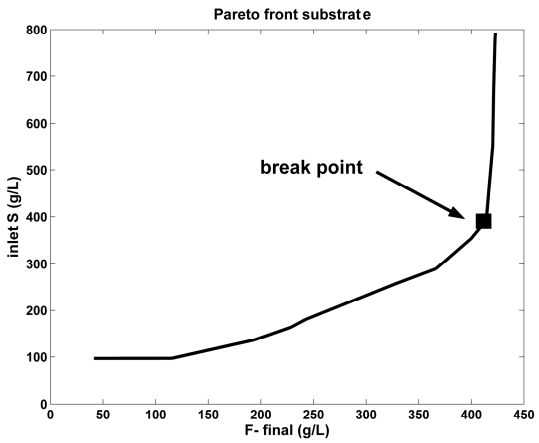

Figure 6. The Pareto-optimal front for the **FBR** (of Table 1) with constant feeding in terms of two opposite objectives, that is, maximum F production vs. minimum substrate (S) consumption. This solution to Equation (3) was obtained by imposing the control variable limits given in Table 6. The set-point was chosen as being the break-point of the Pareto-optimal front, according to the suggestions of Dan and Maria [39].

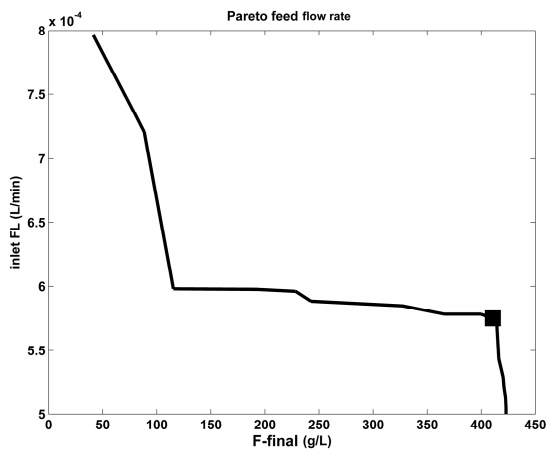

Figure 7. The Pareto-optimal operating policy of the **FBR** (of Table 1) in terms of the required minimum constant feed flow rate, for various maximum F produced. The marked point is the chosen set-point corresponding to those of the Pareto-optimal curve of Figure 6.

4.5. The Used Solvers

During **BR/FBR** optimization, when simulating the reactor dynamics in every solver iteration, the model species bulk-phase concentrations are obtained by solving the dynamic model of the reactor (Table 4 or Table 5, respectively), with the initial condition $c_{j,o}$ (t = 0) being the iterative guess made by the numerical solver. The imposed batch time t_f and the medium conditions are those of Table 1. The dynamic model solution was obtained with high precision by using the variable-order stiff integrator ('ode15s') of the MATLAB (R2010a) package.

Because the differential models of the reactor, the optimization objectives of Equation (1A,B), and the problem constraints Equation (2i–iv) are all highly nonlinear, the Pareto-optimal fronts were obtained by using a multimodal search algorithm, that is, 'gamultiobj' of the MATLAB package. This numerical algorithm is suitable for this non-convex and nonlinear case. The computational time was reasonably short (minutes) using a common PC, thus offering a quick implementation of the optimal **BR** operating policy obtained offline.

Because the enzymatic reactor/process kinetic model (Tables 4 and 5), the optimization objectives of Equation (1A,B), and the problem constraints of Equation (2i–iv) are all highly nonlinear, the formulated problems of Equation (1A,B) translate into a nonlinear optimization problem (**NLP**) with a multimodal objective function and a non-convex searching domain. To obtain the global feasible solution with enough precision, the multimodal optimization solver MMA of Maria [4,99,100] was used, starting from different initial guesses, being proven to be very effective compared to common (commercial) optimization algorithms.

5. Optimization Results and Their Discussion

The results for solving the **NLP** optimization problem are presented in the following forms:

(a) Figure 3 displays the optimal **NLP** operating policy for the analyzed **BR**, by comparison with the experimental data of Ricca et al. [64] obtained in a **BR** operated under non-optimal conditions of Table 2.

(b) A comparison of all **BR** operating alternatives in terms of fructose (F) production and raw-material consumption is in Table 6. In the **BR** case, this consumption is based only on the initial load. In the **FBR** case, the raw-material consumption (mass) is computed with the following formula:

$$m_{species} = \sum_{j=1}^{N_{div}} F_{L,j}[species]_{inlet,j}\,\Delta t_j \quad (4)$$

(c) The optimally operated **FBR**, with a **constant** but optimal NLP feeding in Figure 4.
(d) The optimally operated **FBR** with a **variable** but optimal NLP feeding in Figure 5.

By analyzing these results and, in particular, the operating alternatives of Table 6, several conclusions can be derived:

(1) The optimal **NLP-**operated **BR**, according to Equation (1A), under the constraints of Equation (2i–iv) for the control variables, reported incomparably better performances (5× in terms of more F produced, at the expense of consuming 5× more substrates and 30× more enzymes) compared to the experimental non-optimal **BR** trial of Ricca et al. [64] (in Table 6 and Figure 3).
(2) By far, the best alternative is the **FBR** operated with a **constant** but optimal NLP feeding (Equation (1A)), or operated using the set-point (break-point) given by the Pareto-optimal front, Equation (3). Even if the F-production is similar to those of the optimal **NLP-**operated **BR**, the substrate consumption is 13×–15× lower, by consuming 15×–92× less enzymes (Table 6 and Figure 4). As revealed by the results of Table 6, the **FBR** operated with a **constant**, but using the set-point (break-point) given by the Pareto-optimal front (Equation (3)), under the constraints of Equation (2i–iv) for the control variables, reported the best performances, regarding all the objectives mentioned above.
(3) By analyzing the **FBR** with an optimal NLP *variable feeding*, the results are quite modest. In spite of the realized good F-production, compared to the **FBR** operated with *constant* but Pareto-optimal feeding, the **FBR** with an optimal NLP variable feeding reported higher raw-material consumption (90× more enzymes and 13× more substrates).
(4) Of course, enzyme stabilization by immobilization is expected to improve the process performances, as reviewed in the Introduction section [101].
(5) The optimal **FBR** control strategy is very adaptable, which is because the employed process kinetic model of moderate complexity is flexible enough due to a fairly large number of rate constants. Thus, if significant inconsistencies are observed between the model-predicted bioreactor dynamics and the recorded data, then an intermediate numerical analysis step will be applied to improve the model adequacy (i.e., a 'model updating' step), and the bioreactor optimization is applied again with the novel model. This evolutionary adaptation of the enzymatic process model is the so-called 'tendency modeling' [34].

Table 6. Efficiency of **BR/FBR** (Table 2) operated using various alternatives, for the enzymatic hydrolysis of inulin to fructose, by using a batch time of 780 min for all cases. A total conversion is realized in all the cases.

Reactor Operation				Raw-Material Consumption [b]		Max F (Fructose), (g) [b]	Final VL (L)
Type	N_{div}	Control Variables		S (Inulin), (g) (Equation (4))	E (Enzyme) (U) (Equation (4))		[a]
BR Non-optimal, Ricca et al. [64]	1	Nominal load [c,f] (Figure 4)		40	9.7 (poor)	41.05	1
		[S]o	40				
		[E]o	9.7				
		Wo	988.4				

Table 6. *Cont.*

Reactor Operation				Raw-Material Consumption [b]		Max F (Fructose), (g) [b]	Final VL (L)
Type	N_{div}	Control Variables		S (Inulin), (g) (Equation (4))	E (Enzyme) (U) (Equation (4))		[a]
BR Optimal load NLP (this paper) [h]	1	Initial load [f,b,h] (Figure 3)		200	302 (fairly good)	213.7	2 [g]
		[S]o	200				
		[E]o	301.87				
		Wo	2000				
FBR Constant but optimal NLP feeding (this paper) [d]	1	Optimal feeding [f,j] (Figure 4)		156	2145.9 (almost best)	426.9	1.4
		[S]in	400				
		[E]in	5500				
		FL,in	5×10^{-4}				
FBR Constant but Pareto-optimal feeding (this paper) [d]	1	Optimal feeding [f,j]		180.4	357.9 (best)	422.9	1.4
		[S]in	399.88				
		[E]in	793.19				
		FL,in	5.78×10^{-4}				
FBR Variable optimal NLP feeding (this paper) [e]	5	Optimal feeding [f,j] (Figure 5)		2393.7	3.29×10^4 (high consumptions and dilution)	428	6.98
		[S]in [40–400]	variable Figure 5E				
		[E]in [97–5500]	variable Figure 5D				
		FL,in [5×10^{-4}–0.01]	variable Figure 5C				

Footnotes: [a] Initial liquid volume VL,o = 1 L. [b] The displayed digits come from the numerical simulations. [c] The checked BR set-point of Ricca et al. [64]. [d] The FBR operation with a constant feeding over time for all the control variables (Table 5): $F_{L,1} = F_{L,2} = F_{L,3} = F_{L,4}$; $C_{S,inlet,1} = C_{S,inlet,2} = C_{S,inlet,3} = C_{S,inlet,4}$; $C_{E,inlet,1} = C_{E,inlet,2} = C_{E,inlet,3} = C_{E,inlet,4}$ with the only 3 variables to be optimized being the initial inlet values of $F_{L,1}$, $C_{S,inlet,1}$, and $C_{E,inlet,1}$, under the constraints of Equation (2i–iv). See the resulting optimal FBR operating policy in Figure 4. [e] The optimal FBR time-stepwise variable feeding policy is obtained by using the control variable limits of footnote [j]. In this FBR operating case, the control variables, $F_{L,j}$, $C_{S,inlet,j}$, and $C_{E,inlet,j}$, where j = 1,. . .(Ndiv -1), of Table 5 follow an uneven policy in being optimized (that is, 15 unknowns for Ndiv = 5). The optimal control variable policy is given in Figure 5. [f] The units are as follows: [S] g/L; [E] U/L; [W] g; FL L/min. [g] The volume corresponds to the water (W) mass required by the reaction. [h] Search intervals of the control variables are as follows: [S]in = [40–200] g/L; [E]in = [97–5500] U/L. [j] Search intervals of control variables are as follows: [S]in = [40–400] g/L; [E]in = [97–5500] U/L; FL,in = [5×10^{-4}–0.01] L/min [62].

6. Conclusions

To conclude, with the **BR** operation that was optimized in silico and *offline*, or with an **FBR** with constant but optimal feeding, even though there are simple alternatives to implement, they can offer a significantly improved reactor effectiveness, due to their high flexibility in using an easily adaptable process model, and due to the applied effective optimization rules (single-objective **NLP**).

The nominal, non-optimal **BR** operation used to derive the process kinetic model reported very poor performances. Thus, the same **BR** but optimally **NLP**-operated by also taking into account the technological constraints for the control variables reported incomparably better performances (5× in terms of more fructose produced, at the expense of consuming 5× more substrates and 30× more enzymes).

Our in-silico analysis reveals that, for this enzymatic process, the best alternative is the **FBR** operated with a constant control variable but using the set-point given by the (breakpoint) of the Pareto optimal front of Figure 7, under the imposed technological constraints Equation (2i–iv). This set point reported the best performances, regarding all the considered opposite economic objectives. Also, the **FBR** with a constant, but NLP optimal feeding, reported fairly good performances.

The present optimization analysis proves its worth by including multiple **elements of novelty**: (i) An optimally operated **FBR,** by using wider but feasible ranges for setting the control variables, can lead to high performances of the bioreactor. (ii) The major role played by the biocatalyst (enzyme concentration) as a control variable during **FBR** optimization (an option seldom discussed in the literature). (iii) The in silico (model-based) optimal operation of enzymatic reactors is a very important engineering issue because it can lead to consistent economic benefits, as proven by the results presented in this paper.

Author Contributions: Conceptualization, G.M.; Methodology, G.M.; Software, D.G., G.M. and L.R.; Validation, D.G., G.M., L.R. and C.M.; Formal analysis, D.G., G.M., L.R. and C.M.; Investigation, D.G., G.M., L.R. and C.M.; Data curation, D.G., G.M., L.R. and C.M.; Writing—original draft, D.G., G.M. and L.R.; Writing—review & editing, G.M.; Visualization, D.G., L.R. and C.M.; Supervision, G.M.; Project administration, G.M. All authors have read and agreed to the published version of the manuscript.

Funding: The authors did not receive support from any organization for the submitted work. This research did not receive any specific grant from funding agencies in the public, commercial, or not-for-profit sectors.

Data Availability Statement: Experimental datasets and some information used in this study are imported from the literature, and the source was referred in the text.

Conflicts of Interest: The authors confirm that their paper has no conflict of interest of any kind, and of any nature.

Abbreviations and Notations

c_j	-	species j concentration
K_m, k_2, k_d	-	kinetic model constants
k	-	rate constant vector
M	-	molecular weight
m	-	mass
m	-	fructose degree of polymerization in the inulin
N_{div}	-	number of time arcs, that is, the number of equal divisions of the batch time t_f for an FBR with variable feeding
r_j	-	reaction rate of species j
T	-	temperature
t	-	time
$\Delta\, t$	-	time interval
t_f	-	batch time
V_L, VL	-	liquid volume

Greeks

α, v_{mS}, v_{mF}, v_{mW}, v_{mG}	-	kinetic model constants
Δ	-	finite difference
ν_{ij}	-	the stoichiometric coefficient of species j in reaction i
Ω	-	optimization objective function
ρ	-	density

Index

In, inlet	-	inlet
0,o	-	initial
S, F, W, E, G	-	substrate, fructose, water, enzyme, and glucose, respectively

Abbreviations

BR	-	batch reactor
BRP	-	BR with intermittent addition of enzyme solution
E, ENZ	-	enzyme
F	-	fructose
FBR	-	Fed-batch reactor
G	-	glucose
HFCS	-	high fructose-glucose syrup
HFS	-	high fructose syrup
kDG	-	keto D-glucose (D-glucosone)
Max	-	maximum
NLP	-	nonlinear programming
P2Ox	-	pyranose 2-oxidase
P2Oxox	-	inactive form of P2Ox
S	-	substrate (inulin)
SBR	-	semi-batch reactor
W	-	water

References

1. Moulijn, J.A.; Makkee, M.; van Diepen, A. *Chemical Process Technology*; Wiley: New York, NY, USA, 2001.
2. Wang, P. Multi-scale features in recent development of enzymic biocatalyst systems. *Appl. Biochem. Biotechnol.* **2009**, *152*, 343–352. [CrossRef] [PubMed]
3. Vasić-Rački, D.; Findrik, Z.; Presečki, A.V. Modelling as a tool of enzyme reaction engineering for enzyme reactor development. *Appl. Microbiol. Biotechnol.* **2011**, *91*, 845–856. [CrossRef] [PubMed]
4. Maria, G. A review of algorithms and trends in kinetic model identification for chemical and biochemical systems. *Chem. Biochem. Eng. Q.* **2004**, *18*, 195–222.
5. Gernaey, K.V.; Lantz, A.E.; Tufvesson, P.; Woodley, J.M.; Sin, G. Application of mechanistic models to fermentation and biocatalysis for next-generation processes. *Trends Biotechnol.* **2010**, *28*, 346–354. [CrossRef] [PubMed]
6. Bonvin, D.; Srinivasan, B.; Hunkeler, D. Control and optimization of batch processes. *IEEE Control. Syst. Mag. Dec.* **2006**, 34–45. Available online: https://www.researchgate.net/publication/37426142_Control_and_Optimization_of_Batch_Processes_Improvement_of_Process_Operation_in_the_Production_of_Specialty_Chemicals (accessed on 3 March 2025).
7. Srinivasan, B.; Primus, C.J.; Bonvin, D.; Ricker, N.L. Run-to-run optimization via control of generalized constraints. *Control. Eng. Pract.* **2001**, *9*, 911–919.ec. [CrossRef]
8. Dewasme, L.; Amribt, Z.; Santos, L.O.; Hantson, A.L.; Bogaerts, P.; Wouwer, A.V. Hybridoma cell culture optimization using nonlinear model predictive control. *Int. Fed. Autom. Control.* **2013**, *46*, 60–65. [CrossRef]
9. Dewasme, L.; Cote, F.; Filee, P.; Hantson, A.L.; Wouwer, A.V. Macroscopic dynamic modeling of sequential batch cultures of hybridoma cells: An experimental validation. *Bioengineering* **2017**, *4*, 17. [CrossRef]
10. Mendes, R.; Rocha, I.; Pinto, J.P.; Ferreira, E.C.; Rocha, M. Differential evolution for the offline and online optimization of fed-batch fermentation processes. In *Advances in Differential Evolution*; Studies in Computational Intelligence; Chakraborty, U.K., Ed.; Springer: Berlin/Heidelberg, Germany, 2008; pp. 299–317.
11. Liu, Y.; Gunawan, R. Bioprocess optimization under uncertainty using ensemble modeling. *J. Biotechnol.* **2017**, *244*, 34–44. [CrossRef]
12. Hartig, F.; Keil, F.J.; Luus, R. Comparison of optimization methods for a fed-batch reactor. *Hung. J. Ind. Chem.* **1996**, *23*, 81–160.
13. Amribt, Z.; Dewasme, L.; Wouwer, A.V.; Bogaerts, P. Optimization and robustness analysis of hybridoma cell fed-batch cultures using the overflow metabolism model. *Bioprocess Biosyst. Eng.* **2014**, *37*, 1637–1652. [CrossRef] [PubMed]
14. Bonvin, D. Optimal operation of batch reactors—A personal view. *J. Process Control.* **1998**, *8*, 355–368. [CrossRef]
15. Bonvin, D. *Real-Time Optimization*; MDPI: Basel, Switzerland, 2017.
16. DiBiasio, D. Introduction to the control of biological reactors. In *Chemical Engineering Problems in Biotechnology*; Shuler, M.L., Ed.; American Institute of Chemical Engineers: New York, NY, USA, 1989; pp. 351–391.
17. Abel, O.; Marquardt, W. Scenario-integrated on-line optimisation of batch reactors. *J. Process Control.* **2003**, *13*, 703–715. [CrossRef]
18. Lee, J.; Lee, K.S.; Lee, J.H.; Park, S. An on-line batch span minimization and quality control strategy for batch and semi-batch processes. *Control Eng. Pract.* **2001**, *9*, 901–909. [CrossRef]
19. Ruppen, D.; Bonvin, D.; Rippin, D.W.T. Implementation of adaptive optimal operation for a semi-batch reaction system. *Comput. Chem. Eng.* **1998**, *22*, 185–199. [CrossRef]

20. Loeblein, C.; Perkins, J.; Srinivasan, B.; Bonvin, D. Performance analysis of on-line batch optimization systems. *Comput. Chem. Eng.* **1997**, *21*, S867–S872. [CrossRef]
21. Rao, M.; Qiu, H. *Process Control Engineering: A Textbook for Chemical, Mechanical and Electrical Engineers*; Gordon and Breach Science: Amsterdam, The Netherlands, 1993.
22. Maria, G. Enzymatic reactor selection and derivation of the optimal operation policy, by using a model-based modular simulation platform. *Comput. Chem. Eng.* **2012**, *36*, 325–341. [CrossRef]
23. Maria, G. Model-based optimization of a fed-batch bioreactor for mAb production using a hybridoma cell culture. *Molecules* **2020**, *25*, 5648–5674. [CrossRef]
24. Koutinas, M.; Kiparissides, A.; Pistikopoulos, E.N.; Mantalaris, A. Bioprocess systems engineering: Transferring traditional process engineering principles to industrial biotechnology. *Comput. Struct. Biotechnol. J.* **2012**, *3*, e201210022. [CrossRef]
25. Maria, G. Model-based optimisation of a batch reactor with a coupled bi-enzymatic process for mannitol production. *Comput. Chem. Eng.* **2020**, *133*, 106628–106635. [CrossRef]
26. Wang, C.; Quan, H.; Xu, X. Optimal design of multiproduct batch chemical process using genetic algorithms. *Ind. Eng. Chem. Res.* **1996**, *35*, 3560–3566. [CrossRef]
27. Srinivasan, B.; Bonvin, D.; Visser, E.; Palanki, S. Dynamic optimization of batch processes: II. Role of measurements in handling uncertainty. *Comput. Chem. Eng.* **2003**, *27*, 27–44. [CrossRef]
28. Ozturk, S.S.; Palsson, B.O. Effect of initial cell density on hybridoma growth, metabolism, and monoclonal antibody production. *J. Biotechnol.* **1990**, *16*, 259–278. [CrossRef] [PubMed]
29. Martinez, E. Batch-to-batch optimization of batch processes using the STATSIMPLEX search method. In Proceedings of the 2nd Mercosur Congress on Chemical Engineering, Rio de Janeiro, Costa Verde, Brasil, 14–18 August 2005. paper #20.
30. Engasser, J.M. Bioreactor engineering: The design and optimization of reactors with living cells. *Chem. Eng. Sci.* **1988**, *43*, 1739–1748. [CrossRef]
31. Lübbert, A.; Jørgensen, S.B. Bioreactor performance: A more scientific approach for practice. *J. Biotechnol.* **2001**, *85*, 187–212. [CrossRef]
32. Binette, J.C.; Srinivasan, B. On the use of nonlinear model predictive control without parameter adaptation for batch processes. *Processes* **2016**, *4*, 27. [CrossRef]
33. Maria, G.; Peptanaru, I.M. Model-based optimization of mannitol production by using a sequence of batch reactors for a coupled bi-enzymatic process—A dynamic approach. *Dynamics* **2021**, *1*, 134–154. [CrossRef]
34. Fotopoulos, J.; Georgakis, C.; Stenger, H.G., Jr. Uncertainty Issues in the Modeling and Optimization of Batch Reactors with Tendency Models. *Chem. Eng. Sci.* **1994**, *49*, 5533–5547. [CrossRef]
35. Smets, I.Y.; Claes, J.E.; November, E.J.; Bastin, G.P.; van Impe, J.F. Optimal adaptive control of (bio)chemical reactors: Past, present and future. *J. Process Control.* **2004**, *14*, 795–805. [CrossRef]
36. Maria, G.; Crisan, M. Evaluation of optimal operation alternatives of reactors used for D-glucose oxidation in a bi-enzymatic system with a complex deactivation kinetics. *Asia-Pac. J Chem Eng.* **2014**, *10*, 22–44. [CrossRef]
37. Franco-Lara, E.; Weuster-Botz, D. Estimation of optimal feeding strategies for fed-batch bioprocesses, Estimation of optimal feeding strategies for fed-batch bioprocesses. *Bioprocess Biosyst. Eng.* **2005**, *28*, 71–77. [CrossRef]
38. Maria, G.; Renea, L. Tryptophan production maximization in a fed-batch bioreactor with modified *E. coli* cells, by optimizing its operating policy based on an extended structured cell kinetic model. *Bioengineering* **2021**, *8*, 210–247. [CrossRef] [PubMed]
39. Dan, A.; Maria, G. Pareto Optimal Operating Solutions for a Semibatch Reactor Based on Failure Probability Indices. *Chem. Eng. Technol.* **2012**, *35*, 1098–1103. [CrossRef]
40. Avili, M.G.; Fazaelipoor, M.H.; Jafari, S.A.; Ataei, S.A. Comparison between batch and fed-batch production of rhamnolipid by *Pseudomonas aeruginosai*. *Iran. J. Biotechnol.* **2012**, *10*, 263–269.
41. Koller, M. A review on established and emerging fermentation schemes for microbial production of polyhydroxyalkanoate (PHA) biopolyesters. *Fermentation* **2018**, *4*, 30. [CrossRef]
42. Akinterinwa, O.; Khankal, R.; Cirino, P.C. Metabolic engineering for bioproduction of sugar alcohols. *Curr. Opin. Biotechnol.* **2008**, *19*, 461–467. [CrossRef]
43. Fu, Y.; Ding, L.; Singleton, M.L.; Idrissi, H.; Hermans, S. Synergistic effects altering reaction pathways: The case of glucose hydrogenation over Fe-Ni catalysts. *Appl. Catal. B Environ.* **2021**, *288*, 119997. [CrossRef]
44. Ahmed, M.J.; Hameed, B.H. Hydrogenation of glucose and fructose into hexitols over heterogeneous catalysts, A review. *J. Taiwan Inst. Chem. Eng.* **2019**, *96*, 341–352. [CrossRef]
45. Liese, A.; Seelbach, K.; Wandrey, C. (Eds.) *Industrial Biotransformations*; Wiley-VCH: Weinheim, Germany, 2006.
46. Myande Comp. Fructose Syrup Production, China. 2024. Available online: https://www.myandegroup.com/starch-sugar-technology?ad_account_id=755-012-8242&gad_source=1 (accessed on 3 March 2025).
47. Marianou, A.A.; Michailof, C.M.; Pineda, A.; Iliopoulou, E.F.; Triantafyllidis, K.S.; Lappas, A.A. Glucose to fructose isomerization in aqueous media over homogeneous and heterogeneous catalysts. *ChemCatChem* **2016**, *8*, 1100–1110. [CrossRef]

48. Hanover, L.M.; White, J.S. Manufacturing, composition, and applications of fructose. *Am. J. Clin. Nutr.* **1993**, *58*, 724S–732S. [CrossRef]
49. Leitner, C.; Neuhauser, W.; Volc, J.; Kulbe, K.D.; Nidetzky, B.; Haltrich, D. The Cetus process revisited: A novel enzymatic alternative for the production of aldose-free D-fructose. *Biocatal. Biotransform.* **1998**, *16*, 365–382. [CrossRef]
50. Shaked, Z.; Wolfe, S. Stabilization of pyranose 2-oxidase and catalase by chemical modification. *Methods Enz.* **1988**, *137*, 599–615. Available online: http://www.eng.tau.ac.il/~brauner/Workshop08Participant/Example-7/Prob-14-13.pdf (accessed on 3 March 2025).
51. Maria, G.; Ene, M.D.; Jipa, I. Modelling enzymatic oxidation of D-glucose with pyranose 2-oxidase in the presence of catalase. *J. Mol. Catal. B Enzym.* **2012**, *74*, 209–218. [CrossRef]
52. Bannwarth, M.; Heckmann-Pohl, D.; Bastian, S.; Giffhorn, F.; Schulz, G.E. Reaction geometry and thermostable variant of pyranose 2-oxidase from the white-rot fungus *Peniophora* sp. *Biochemistry* **2006**, *45*, 6587–6595. [CrossRef]
53. Maria, G.; Ene, M.D. Modelling enzymatic reduction of 2-keto-D-glucose by suspended aldose reductase. *Chem. Biochem. Eng. Q.* **2013**, *27*, 385–395.
54. Chenault, H.K.; Whitesides, G.M. Regeneration of nicotinamide cofactors for use in organic synthesis. *Appl. Biochem. Biotechnol.* **1987**, *14*, 147–197. [CrossRef]
55. Parmentier, S.; Arnaut, F.; Soetaert, W.; Vandamme, E.J. Enzymatic production of D-mannitol with the Leuconostoc pseudomesenteroides mannitol dehydrogenase coupled to a coenzyme regeneration system. *Biocatal. Biotransform.* **2005**, *23*, 1–7. [CrossRef]
56. Gijiu, C.L.; Maria, G.; Renea, L. Pareto optimal operating policies of a batch bi-enzymatic reactor for mannitol production. *Chem. Eng. Technol.* **2024**, *48*, e202300555. [CrossRef]
57. Leonida, M.D. Redox enzymes used in chiral syntheses coupled to coenzyme regeneration. *Curr. Med. Chem.* **2001**, *8*, 345–369. [CrossRef]
58. Liu, W.; Wang, P. Cofactor regeneration for sustainable enzymatic biosynthesis. *Biotechnol. Adv.* **2007**, *25*, 369–384. [CrossRef]
59. Berenguer-Murcia, A.; Fernandez-Lafuente, R. New trends in the recycling of NAD(P)H for the design of sustainable asymmetric reductions catalyzed by dehydrogenases. *Curr. Org. Chem.* **2010**, *14*, 1000–1021. [CrossRef]
60. Ghoreishi, S.M.; Shahrestani, R.G. Innovative strategies for engineering mannitol production. *Trends Food Sci. Technol.* **2009**, *20*, 263–270. [CrossRef]
61. Roberfroid, M. *Inulin-Type Fructans*; CRC Press: Boca Raton, FL, USA, 2005.
62. Ricca, E.; Calabro, V.; Curcio, S.; Iorio, G. The state of the art in the production of fructose from inulin enzymatic hydrolysis. *Crit. Rev. Biotechnol.* **2007**, *27*, 129–145. [CrossRef]
63. Ricca, E.; Calabro, V.; Curcio, S.; Iorio, G. Fructose production by chicory inulin enzymatic hydrolysis: A kinetic study and reaction mechanism. *Process Biochem.* **2009**, *44*, 466–470. [CrossRef]
64. Ricca, E.; Calabrò, V.; Curcio, S.; Iorio, G. Optimization of inulin hydrolysis by inulinase accounting for enzyme time- and temperature-dependent deactivation. *Biochem. Eng. J.* **2009**, *48*, 81–86. [CrossRef]
65. Dıaz, E.G.; Catana, R.; Ferreira, B.S.; Luque, S.; Fernandes, P.; Cabral, J.M.S. Towards the development of a membrane reactor for enzymatic inulin hydrolysis. *J. Membr. Sci.* **2006**, *273*, 152–158. [CrossRef]
66. Rocha, J.R.; Catana, R.; Ferreira, B.S.; Cabral, J.M.S.; Fernandes, P. Design and characterisation of an enzyme system for inulin hydrolysis. *Food Chem.* **2006**, *95*, 77–82. [CrossRef]
67. Phelps, C.F. The physical properties of inulin solutions. *Biochem. J.* **1965**, *95*, 41–47. [CrossRef]
68. Toneli, J.T.C.L.; Park, K.J.; Murr, F.E.X.; Martinelli, P.O. Rheological bahavior of concentrated inulin solution: Influence of soluble solids concentration and temperature. *J. Texture Stud.* **2008**, *39*, 369–392. [CrossRef]
69. Bot, A.; Erle, U.; Vreeker, R.; Agterof, W.G.M. Influence of crystallisation conditions on the large deformation rheology of inulin gels. *Food Hydrocoll.* **2004**, *18*, 547–556. [CrossRef]
70. Bendayan, M.; Rasio, E.A. Transport of insulin and albumin by the microvascular endothelium of the rete mirabile. *J. Cell Sci.* **1996**, *109*, 1857–1864. [CrossRef] [PubMed]
71. Silva, A.T.C.R. Fructose solubility in water and ethanol/water. In Proceedings of the AIChE Meeting, Tampa, FL, USA, 8–13 November 2009; p. 1543.
72. Chen, J.C.P.; Chou, G.C. *Chen-Chou Cane Sugar Handbook*; Wiley: New York, NY, USA, 1993; p. 24.
73. Okutomi, T.; Nemoto, M.; Mishiba, E.; Goto, F. Viscosity of diluent and sensory -level of subarachnoid anaesthesia achieved with tetracaine. *Can. J. Anesth.* **1998**, *45*, 84–86. [CrossRef]
74. Giordano, R.L.C.; Giordano, R.C.; Cooney, C.L. A study on intra-particle diffusion effects in enzymatic reactions: Glucose-fructose isomerisation. *Bioprocess Eng.* **2000**, *23*, 159–166. [CrossRef]
75. Santos, A.M.P.; Oliveira, M.G.; Maugeri, F. Modelling thermal stability and activity of free and immobilized enzymes as a novel tool for enzyme reactor design. *Bioresour. Technol.* **2007**, *98*, 3142–3148. [CrossRef] [PubMed]

76. Catana, R.; Eloy, M.; Rocha, J.R.; Ferreira, B.S.; Cabral, J.M.S.; Fernandes, P. Stability evaluation of an immobilized enzyme system for inulin hydrolysis. *Food Chem.* **2007**, *101*, 260–266. [CrossRef]
77. Kim, W.Y.; Byun, S.M.; Uhm, T.B. Hydrolysis of inulin from Jerusalem artichoke by inulinase immobilized on aminoethylcellulose. *Enzym. Microb. Technol.* **1982**, *4*, 239–244. [CrossRef]
78. Kim, C.H.; Rhee, S.K. Fructose production from Jerusalem artichoke by inulinase immobilized on chitin. *Biotechnol. Lett.* **1989**, *11*, 201–206. [CrossRef]
79. Nakamura, T.; Ogata, Y.; Shitara, A.; Nakamura, A.; Ohta, K. Continuous Production of Fructose Syrups from Inulin by Immobilized Inulinase from Aspergillus niger Mutant 817. *Jl. Ferment. Bioeng.* **1995**, *80*, 164–169. [CrossRef]
80. Yun, J.W.; Kim, D.H.; Kim, B.W.; Song, S.K. Production of inulo-oligosaccharides from inulin by immobilized endoinulinase from Pseudomonas sp. *J. Ferment. Bioeng.* **1997**, *84*, 369–371. [CrossRef]
81. Gupta, A.K.; Singh, D.P.; Kaur, N.; Singh, R. Production, purification and immobilisation of inulinase from Kluyveromyces fragilis. *J. Chem. Tech. Biotechnol.* **1994**, *59*, 377–385. [CrossRef]
82. Wenling, W.; Huiying, W.W.L.; Shiyuan, W. Continuous preparation of fructose syrups from Jerusalem artichoke tuber using immobilized intracellular inulinase from *Kluyveromyces* sp. Y-85. *Process Biochem.* **1999**, *34*, 643–646. [CrossRef]
83. Workman, W.E.; Day, D.F. Enzymatic hydrolysis of inulin to fructose by glutaraldehyde fixed yeast cells. *Biotechnol. Bioeng.* **1984**, *26*, 905–910. [CrossRef]
84. Akbas, M.Y.; Stark, B.C. Recent trends in bioethanol production from food processing byproducts. *J. Ind. Microbiol. Biotechnol.* **2016**, *43*, 1593–1609. [CrossRef] [PubMed]
85. Tewari, Y.B.; Goldberg, R.N. Thermodynamics of the conversion of aqueous glucose to fructose. *Appl. Biochem. Biotechnol.* **1985**, *11*, 17–24. [CrossRef]
86. Illanes, A.; Zúñiga, M.E.; Contreras, S.; Guerrero, A. Reactor design for the enzymatic isomerization of glucose to fructose. *Bioprocess Biosyst. Eng.* **1992**, *7*, 199–204. [CrossRef]
87. Lee, H.S.; Hong, J. Kinetics of glucose isomerization to fructose by immobilized glucose isomerase: Anomeric reactivity of D-glucose in kinetic model. *J. Biotechnol.* **2000**, *84*, 145–153. [CrossRef]
88. Straathof, A.J.J.; Adlercreutz, P. *Applied Biocatalysis*; Harwood Academic Publisher: Amsterdam, The Netherlands, 2005.
89. Dehkordi, A.M.; Safari, I.; Karima, M.M. Experimental and modeling study of catalytic reaction of glucose isomerization: Kinetics and packed-bed dynamic modelling. *AIChE J.* **2008**, *54*, 1333–1343. [CrossRef]
90. Bishop, M. *An Introduction to Chemistry*; Chiral Publisher: Raleigh, NC, USA, 2013. Available online: https://preparatorychemistry.com/Bishop_contact.html (accessed on 3 March 2025).
91. Laos, K.; Harak, M. The viscosity of supersaturated aqueous glucose, fructose and glucose-fructose solutions. *J. Food Phys.* **2014**, *27*, 27–30.
92. Viet Bui, A.; Nguyen, M.H. Prediction of viscosity of glucose and calcium chloride solutions. *J. Food Eng.* **2004**, *62*, 345–349.
93. Maria, G.; Renea, L.; Gheorghe, D. In-Silico optimization of a FBR for ethanol production by using several algorithms and operating alternatives. *Rev. Roum. Chim.* **2024**, *70*. *in press*.
94. Moser, A. *Bioprocess Technology—Kinetics and Reactors*; Springer: Berlin/Heidelberg, Germany, 1988.
95. Dutta, R. *Fundamentals of Biochemical Engineering*; Springer: Berlin/Heidelberg, Germany, 2008.
96. Maria, G.; Renea, L.; Maria, C. Multi-objective optimization of the fed-batch bi-enzymatic reactor for mannitol production. *Dynamics* **2022**, *2*, 270–294. [CrossRef]
97. Rao, S.S. *Engineering Optimization—Theory and Practice*; Wiley: New York, NY, USA, 2009; Chapter 14.10.
98. Dan, A.; Maria, G. Pareto optimal operating solutions for a catalytic reactor for butane oxidation based on safety indices. *U.P.B. Sci. Bull. Series B—Chemie* **2014**, *76*, 35–48. Available online: http://www.scientificbulletin.upb.ro/ (accessed on 3 March 2025).
99. Maria, G. Adaptive Random Search and Short-Cut Techniques for Process Model Identification and Monitoring. *AIChE Symp. Ser.* **1998**, *94*, 351–359.
100. Maria, G. ARS combination with an evolutionary algorithm for solving MINLP optimization problems. In *Modelling, Identification and Control*; Hamza, M.H., Ed.; IASTED/ACTA Press: Anaheim, CA, USA, 2003; pp. 112–118.
101. Bickerstaff, G.F. (Ed.) *Immobilization of Enzymeas and Cells*; Humana Press Inc.: Totowa, NJ, USA, 1997.